Slip effects on streamline topologies and their bifurcations for peristaltic flows of a viscous fluid

Z. Asghar† and N. Ali

Department of Mathematics and Statistics, International Islamic University, Islamabad 44000, *Pakistan*

(Received 5 September 2013; revised manuscript received 30 October 2013; published online 20 April 2014)

We discuss the effects of the surface slip on streamline patterns and their bifurcations for the peristaltic transport of a Newtonian fluid. The flow is in a two-dimensional symmetric channel or an axisymmetric tube. An exact expression for the stream function is obtained in the wave frame under the assumptions of long wavelength and low Reynolds number for both cases. For the discussion of the particle path in the wave frame, a system of nonlinear autonomous differential equations is established and the methods of dynamical systems are used to discuss the local bifurcations and their topological changes. Moreover, all types of bifurcations and their topological changes are discussed graphically. Finally, the global bifurcation diagram is used to summarize the bifurcations.

Keywords: viscous fluid, slip condition, streamline topologies, bifurcation

PACS: 47.15.−X, 47.10.ad, 47.15.G−, 05.45.−a **DOI:** 10.1088/1674-1056/23/6/064701

1. Introduction

Peristaltic motion is simply a form of material transport induced by the progressive wave of area contraction or expansion along the longitudinal direction of a flexible tube or channel. This motion occurs in many biological systems, such as the transport of urine from the kidney to the bladder, the transport of spermatozoa in vas deferens, food mixing, and chymes movement in the intestine, the transport of bile in the bile duct, and the circulation of blood in small blood vessels. Some modern mechanical devices have been designed on the principle of peristaltic pumping for transporting fluids without contact to internal moving parts.

In the pioneer works on peristaltic transport, investigations were performed for urine transport, and the continuity and Navier–Stokes equations were used as a mathematical model of the problem. Mention may be made to Ref. [1], in which the author analyzed the peristaltic pumping in a two-dimensional flexible tube. He had taken the assumptions of a small wave number and an inertia free flow for the simplification of the problem. Under those assumptions, the flow was steady in the wave frame and the calculated exact solution was the well-known velocity profile of the Poiseuille flow. The theoretical results obtained[1] were later confirmed experimentally.[2,3] In Ref. [4], the peristaltic transport of Newtonian fluid in a planar channel and in a circular tube was investigated. In addition to the long wavelength approximation, the authors also adopted the assumption of low Reynolds number. Besides those studies, many contributions on the peristaltic transport of real fluids were reported in the literature, which incorporate the effects of curvature, MHD, slip effects, and heat/mass transfer analysis, etc.[5–22]

Most investigations on peristalsis include a discussion of the trapping phenomenon, and this phenomenon is associated with streamline patterns, which play a vital role in describing the important flow features. Since peristaltic transport shows an appealing topology of flow, therefore it seems natural to analyze streamline patterns and their bifurcations from the topological point of view with the help of methods of dynamical systems. From a literature review, we come to know that the qualitative approach on streamline patterns using the theory of dynamical systems is not a new idea in the field of fluid dynamics, because a number of contributions have been made in the past. Particularly, the early work on separation was done in Refs. [23]–[26]. In Ref. [22], the discussion on the flow around obstacles was made by applying the topology to flow visualization. Qualitative approaches in analyzing the streamline patterns could also be found in Refs. [27] and [28]. In Ref. [29], the streamline topologies and their bifurcations were analyzed near simple degenerate critical points for a two-dimensional viscous incompressible flow away from the boundaries. The normal form coefficients were used to discuss the bifurcations. Such a study was also performed near a non-simple degenerate critical point close to the stationary wall in Ref. [30].

It would not be wrong to say that the qualitative approach to study streamline behaviors and their bifurcations for peristaltic flows is quite a new area of research and was initiated in Ref. [31]. By this approach, one can find the limits of the flow rates for the backward flow region, the trapping, and the augmented flow region. Moreover, one can also locate different positions (stagnation points) in the flow field where vortices or eddying motion occur or where the separatrices are the divid-

†Corresponding author. E-mail: zaheer_asghar@yahoo.com

© 2014 Chinese Physical Society and IOP Publishing Ltd

ing streamlines. A number of investigations on the peristaltic transport reported a phenomenon of trapping and they highlighted that the size of the trapped bolus increases/decreases with the variations of some of the parameters of interest. Here it is important to mention that no one has yet probed the fact behind that decay or increase in the size of the trapped bolus. It is the qualitative approach to study the streamlines pattern that enables one to explicitly provide the facts.

Motivated by the above discussion, we extend the results in Ref. [31] by analyzing the streamline topologies and their bifurcations under the effects of a surface slip. By surveying the literature on peristaltic transport, we find that the size of the trapped bolus decreases with increasing slip parameter. The present work will provide physical reasons behind the decay in the size of the trapped bolus. This paper is organized as follows. Section 2 presents the formulation of the problem both for planar and axisymmetric flows. A dynamical system approach is used to investigate the nature and the bifurcations of the critical points. Global bifurcations and streamline patterns are also discussed in this section. The results are presented in Section 3. Section 4 reports on the major findings of the analysis.

2. Problem formulation

2.1. Channel flow

Consider the peristaltic transport of an incompressible viscous fluid in a two-dimensional channel of width $2a$. The flow is initiated by the sinusoidal wave trains propagating on the channel walls with constant speed c. The shape of the wall surface is characterized by the same expression as in Ref. [27]

$$\overline{H}(\overline{X},\bar{t}) = R_{\rm w} - a\left[1-\cos^2\left(\frac{\pi}{\lambda}(\overline{X}-c\bar{t})\right)\right], \tag{1}$$

where $R_{\rm w}$ is the average height of the channel from the initial horizontal line, a is the amplitude of the wave, λ is the wavelength, c is the wave speed, and $(\overline{X},\overline{Y})$ are the rectangular coordinates with the $\overline{X}$ axis along the channel and the $\overline{Y}$ axis transverse to the channel.

The Cauchy stress tensor ($\overline{\boldsymbol{T}}$) for the viscous fluid is

$$\overline{\boldsymbol{T}} = -\overline{P}\overline{\boldsymbol{I}} + \mu\overline{\boldsymbol{A}}_1, \tag{2}$$

where μ is the viscosity, $\overline{P}$ is the pressure, and $\overline{\boldsymbol{I}}$ is the identity tensor. The first Rivillin–Ericksen tensor ($\overline{\boldsymbol{A}}_1$) is defined by

$$\overline{\boldsymbol{A}}_1 = \left(\mathrm{grad}\overline{\boldsymbol{V}}\right) + \left(\mathrm{grad}\overline{\boldsymbol{V}}\right)^{\rm T}, \tag{3}$$

where $\overline{\boldsymbol{V}}$ is the fluid velocity vector, and T represents the transpose. The governing equations can be written in the laboratory frame $(\overline{X},\overline{Y})$ as

$$\frac{\partial\overline{U}}{\partial\overline{X}} + \frac{\partial\overline{V}}{\partial\overline{Y}} = 0, \tag{4}$$

$$\rho\left(\frac{\partial}{\partial\bar{t}} + \overline{U}\frac{\partial}{\partial\overline{X}} + \overline{V}\frac{\partial}{\partial\overline{Y}}\right)\overline{U} = -\frac{\partial\overline{P}}{\partial\overline{X}} + \mu\left(\frac{\partial^2\overline{U}}{\partial\overline{X}^2} + \frac{\partial^2\overline{U}}{\partial\overline{Y}^2}\right), \tag{5}$$

$$\rho\left(\frac{\partial}{\partial\bar{t}} + \overline{U}\frac{\partial}{\partial\overline{X}} + \overline{V}\frac{\partial}{\partial\overline{Y}}\right)\overline{V} = -\frac{\partial\overline{P}}{\partial\overline{Y}} + \mu\left(\frac{\partial^2\overline{V}}{\partial\overline{X}^2} + \frac{\partial^2\overline{V}}{\partial\overline{Y}^2}\right), \tag{6}$$

where ρ is the fluid density, $\overline{U}$ and $\overline{V}$ are the respective the velocity components in $\overline{X}$ and $\overline{Y}$ directions, and $\bar{t}$ is the time.

The unsteady flow in the laboratory frame $(\overline{X},\overline{Y})$ can be treated as steady in the coordinate system $(\bar{x},\bar{y})$ moving with wave speed c. The relations between coordinates, velocities, and pressures in the two frames are given by

$$\begin{aligned} &\bar{x} = \overline{X} - c\bar{t}, \quad \bar{y} = \overline{Y}, \quad \bar{u} = \overline{U} - c, \quad \bar{v} = \overline{V}, \\ &\overline{p}(\bar{x},\bar{y}) = \overline{P}(\overline{X},\overline{Y},\bar{t}). \end{aligned} \tag{7}$$

In the above expressions, $\bar{u}$, $\bar{v}$, and $\overline{p}$ represent the velocity components and the pressure in the wave frame, respectively. By making use of the dimensionless variables

$$\begin{aligned} &x = \frac{\pi\bar{x}}{\lambda}, \ y = \frac{\bar{y}}{R_{\rm w}}, \ u = \frac{\bar{u}}{c}, \ v = \frac{\bar{v}}{c\epsilon}, \ t = \frac{\pi c\bar{t}}{\epsilon}, \\ &p = \frac{\epsilon R_{\rm w}\overline{p}}{\mu c}, \ h = \frac{\overline{h}}{R_{\rm w}}, \end{aligned} \tag{8}$$

and defining the stream function through

$$u = \frac{\partial\psi}{\partial y}, \ v = -\frac{\partial\psi}{\partial x}, \tag{9}$$

equation (4) is identically satisfied, whereas the Navier–Stokes equations (5) and (6) after the cross differentiation for eliminating the pressure gradient take the form

$$Re\epsilon\left[\psi_y\nabla^2\psi_x - \psi_x\nabla^2\psi_y\right] = \nabla^2(\nabla^2\psi). \tag{10}$$

In non-dimensional form, equation (1) reduces to

$$h(x) = 1 - \phi\left(1-\cos^2 x\right). \tag{11}$$

In Eqs. (10) and (11), the wave number ϵ, the Reynolds number Re, the kinematic viscosity ν, the amplitude ratio ϕ, and the modified Laplacian ∇^2 are defined by the relations

$$\begin{aligned} &\epsilon = \frac{\pi R_{\rm w}}{\lambda}, \ Re = \frac{\rho c R_{\rm w}}{\mu}, \ \nu = \frac{\mu}{\rho}, \ \phi = \frac{a}{R_{\rm w}}(<1), \\ &\nabla^2 = \epsilon^2\frac{\partial^2}{\partial x^2} + \frac{\partial^2}{\partial y^2}. \end{aligned} \tag{12}$$

After taking into account the long wavelength and the low Reynolds number assumptions, equation (10) reduces to an analogous equation as obtained in Ref. [31]

$$\frac{\partial^4\psi}{\partial y^4} = 0. \tag{13}$$

The dimensionless volume flow rate and boundary conditions in the wave frame are

$$\psi = 0, \ \frac{\partial^2\psi}{\partial y^2} = 0, \ \text{at} \ y = 0, \tag{14a}$$

$$\psi = q, \quad \frac{\partial \psi}{\partial y} + \beta \frac{\partial^2 \psi}{\partial y^2} = -1, \quad \text{at } y = h, \tag{14b}$$

$$q = \int_0^h \frac{\partial \psi}{\partial y} \mathrm{d}y = \psi(h) - \psi(0). \tag{15}$$

Here β ($= \eta / R_{\mathrm{w}}$, η is the dimensional slip parameter) is the dimensionless slip parameter, h is the dimensionless form of the peristaltic wall, and q is the dimensionless mean flow rate in the wave frame. Since the flow is symmetric with respect to the centerline, therefore we shall discuss the problem in the domain $y \in [0, h]$.

2.1.1. Solution of the problem

The solution of Eq. (13) subject to boundary conditions (14a) and (14b) is

$$\psi = \frac{1}{h}\left(\frac{3qh + h^2 + 6\beta q}{2h + 6\beta}\right) y - \left(\frac{q + h}{2h^3 + 6\beta h^2}\right) y^3. \tag{16}$$

Three different flow situations, namely, backward flow, trapping, and augmented flow, occur. The backward flow refers to the case in which the whole flow goes in the direction opposite to the traveling wave. The trapping is the situation where the streamline splits to enclose an amount of fluid, called a bolus. The augmented flow occurs when the trapped bolus splits and there exist some flows going in the forward direction.

2.1.2. Flow field as a nonlinear dynamical system

In this section, we employ the idea of the qualitative theory of dynamical systems. At a particular instant, say t_0, the motion of individual particles moving in a path defined by $\dot{x} = [u(x,y,t), v(x,y,t), 0]$ is identical to the instantaneous streamlines, in other words, we have $\dot{x} = [u(x,y,t_0), v(x,y,t_0), 0]$. The present problem can be written as a system of following nonlinear differential equations by using the relations $u(x,y) = \partial \psi / \partial y$, $v(x,y) = -\partial \psi / \partial x$, and Eq. (16):

$$\dot{x} = \frac{3qh + h^2 + 6\beta q}{2h^2 + 6\beta h} - \frac{(3y^2)(q + h)}{2h^3 + 6\beta h^2} = f(x, y, \boldsymbol{\alpha}), \tag{17}$$

$$\begin{aligned} \dot{y} &= y \frac{\partial h}{\partial x} \frac{1}{h(2h^2 + 6\beta h)^2} \left[6qh(h^2 - y^2) - 4h^2 y^2 \right. \\ &\quad \left. - 6\beta h(h^2 + y^2) + 12\beta q(2h^2 - y^2)\right] + 36\beta^2 qh \\ &= g(x, y, \boldsymbol{\alpha}), \end{aligned} \tag{18}$$

where $\boldsymbol{\alpha} = [\phi, q, \beta]$, $-\infty < x < \infty$, $-h < y < h$, and the amplitude ratio ϕ lies between 0 and 1.

To obtain the critical points, we set $f(x, y, \boldsymbol{\alpha}) = 0 = g(x, y, \boldsymbol{\alpha})$ by following Ref. [31] and then use the Hartman–Grobman theorem, according to which the nature of the critical point can be found by using the Jacobian at the critical point. If the determinant of the Jacobian at a certain critical point is zero, the critical point is degenerate. There are two subclasses of degeneracies called simple and non-simple. A simple degeneracy corresponds to the case when the eigenvalues of the Jacobian are zero. For a non-simple degeneracy, the Jacobian is a zero matrix. We shall use the notation[32] to classify the critical points, where the trace $p_{12} = \lambda_1 + \lambda_2$ and the Jacobian $d_{12} = \lambda_1 \lambda_2$, which are based on eigenvalues λ_1 and λ_2, are used to classify the phase portraits.

According to Ref. [33], a bifurcation point with respect to parameter $\boldsymbol{\alpha}$ is a solution $(x, y, \boldsymbol{\alpha})$, where the number of equilibria, periodic or quasi-periodic solutions change when $\boldsymbol{\alpha}$ passes through $\boldsymbol{\alpha}_{\mathrm{c}}$, with α_{c} as a critical value.

The critical points are given by

i) $\{x_{1,2}, y_{1,2}\} = \left\{ n\pi, \pm \sqrt{\frac{3q + 1 + 6\beta q}{3(q+1)}} \right\}$,

ii) $\{x_{3,4}, y_{3,4}\} = \left\{ \pm \cos^{-1} \sqrt{\frac{\phi - 1 - \frac{3q}{2} - \frac{1}{2}\sqrt{9q^2 - 24\beta q}}{\phi}}, 0 \right\}$,

iii) $\{x_{5,6}, y_{5,6}\} = \left\{ \frac{(2n-1)\pi}{2}, \right.$
$\left. \pm \sqrt{\frac{(3q + 1 - \phi)(1 - \phi)^2 + 6\beta q(1 - \phi)}{3(q + 1 - \phi)}} \right\}$.

In the coming sections, we shall present the qualitative classification and discussion on the critical points. We will also discuss the critical values of the parameters and show the graphical representations of the local and global bifurcations of the critical points.

2.1.3. Classification and bifurcation of the critical points

The critical points

$$\{x_{1,2}, y_{1,2}\} = \left\{ n\pi, \pm \sqrt{\frac{3q + 1 + 6\beta q}{3(q+1)}} \right\},$$

where $n \in \mathbb{Z}$, lie vertically below the wave crests. The Jacobian at these critical points is

$$J|_{\{x_{1,2}, y_{1,2}\}} = \begin{bmatrix} 0 & \mp \frac{3(q+1)}{1+3\beta} \sqrt{\frac{3q+1+6\beta q}{3(q+1)}} \\ \left(\pm \frac{\phi(3q+2+3\beta+6\beta q)}{(1+3\beta)^2} \left(\sqrt{\frac{3q+1+6\beta q}{3(q+1)}} \right)^3 \mp \frac{\phi(3q-3\beta+12\beta q+18\beta^2 q)}{(1+3\beta)^2} \left(\sqrt{\frac{3q+1+6\beta q}{3(q+1)}} \right) \right) & 0 \end{bmatrix}, \tag{19}$$

and the eigenvalues of the Jacobian are given by

$$\lambda_{1,2} = \pm \frac{\sqrt{6\phi(q+1)(3q+1+6\beta q)(1+3\beta)(1+6\beta-9\beta q^2-18\beta^2 q)}}{3(q+1)(1+3\beta)^2}. \tag{20}$$

Since the eigenvalues vary with q at fixed values of ϕ and β, therefore, the nature and stability of the critical points change with the flow rate q, and the flow rate is taken to be between -1 and 1. Qualitative changes are divided into two cases as follows.

Case 1 $(0 < \beta \leq 1/6)$

(i) As $p_{12} = 0$ and $d_{12} < 0$ when $-1 < q < -1/(3+6\beta)$, therefore the critical point is a co-dimension-two saddle as it depends on β and q; see Fig. 1(a).

(ii) An isolated critical point occurs at $q = q_{c_1} = -1/(3+6\beta)$, which is also known as a degenerate point but it is non-hyperbolic as defined in Ref. [34], because both the eigenvalues and the Jacobian matrix are zero. Moreover, the critical point with $q = -1/(3+6\beta)$ corresponds to non-simple degeneracy because $J|_{\{x_{1,2},y_{1,2}\}} = 0$ for $q = q_{c_1} = -1/(3+6\beta)$; see Fig. 1(a).

(iii) As $p_{12} = 0$ and $d_{12} > 0$ when $q > -1/(3+6\beta)$, therefore each critical point is a center; see Fig. 1(a).

A bifurcation diagram in the q–y plane is shown in Fig. 1(a). In this case, the bifurcation points are at $x = n\pi$ for $n \in \mathbb{Z}$, and are co-dimension-two due to their dependences on two parameters q and β.

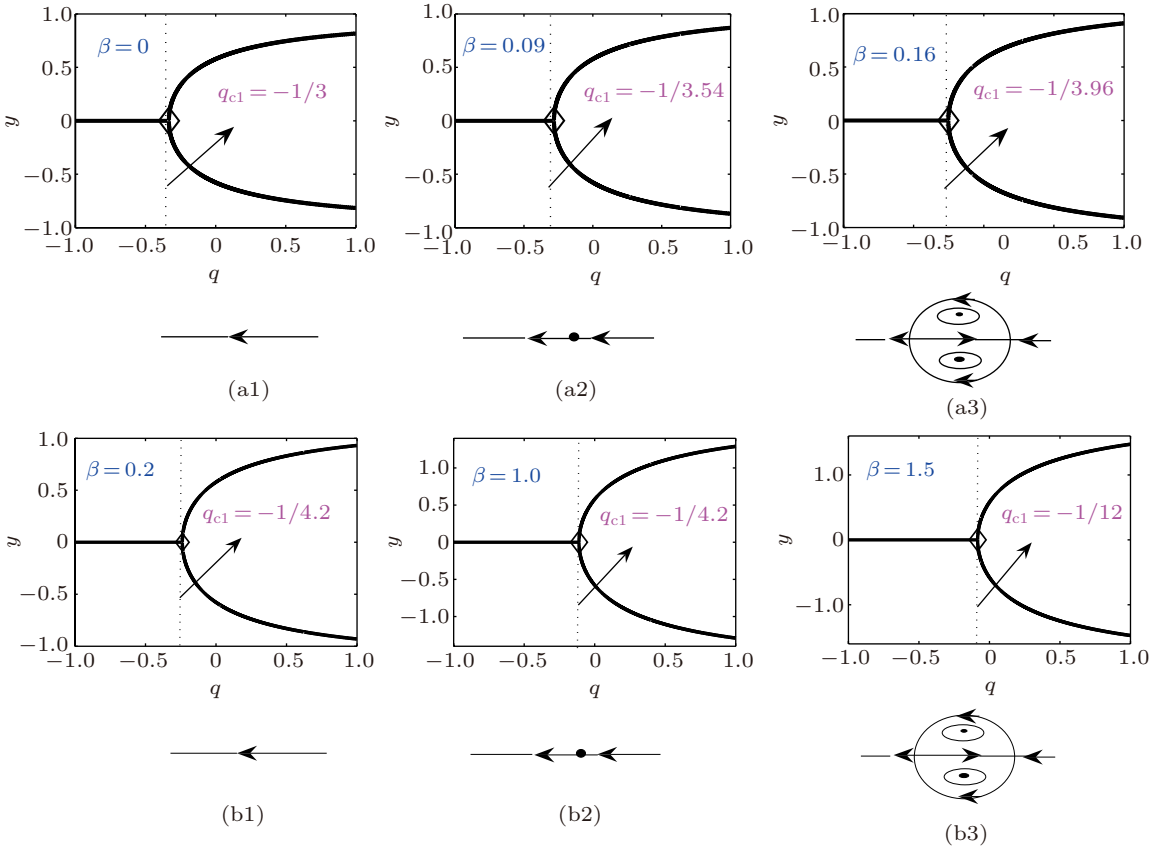


Fig. 1. (color online) (a) Bifurcation diagram for $x = n\pi$, $n \in \mathbb{Z}$ and pictorial topological changes with the variation of β for $0 \leq \beta \leq 1/6$: (a1) $q < -1/(3+6\beta)$, (a2) $q = -1/(3+6\beta)$, (a3) $q > -1/(3+6\beta)$. (b) Bifurcation diagram for $x = n\pi$, $n \in \mathbb{Z}$ and pictorial topological changes with the variation of β for $\beta > 1/6$: (b1) $q < -1/(3+6\beta)$, (b2) $q = -1/(3+6\beta)$, (b3) $q > -1/(3+6\beta)$.

Case 2 (for $\beta > 1/6$)

(I) As $p_{12} = 0$ and $d_{12} < 0$ when $-1 < q < -1/(3+6\beta)$ or $-\beta + 1/3\sqrt{(1+6\beta+9\beta^3)/\beta} < q < 1$, therefore the critical point is a co-dimensional-two saddle as it depends on β and q; see Fig. 1(b).

(II) Isolated critical points occur when $q = q_{c_1} = -1/(3+6\beta)$ and $q = q_{c_2} = -\beta + 1/3\sqrt{(1+6\beta+9\beta^3)/\beta}$. These are also known as degenerate points and the degeneracy is non-simple. The critical points are also non-hyperbolic, see Fig. 1(b).

(III) As $p_{12} = 0$ and $d_{12} > 0$ when $-1/(3+6\beta) < q < -\beta + 1/3\sqrt{(1+6\beta+9\beta^3)/\beta}$, therefore each critical point is a center; see Fig. 1(b).

A bifurcation diagram in the q–y plane is shown in Fig. 1(b) and the bifurcation points are also co-dimension two for this case.

2.1.4. Classification and bifurcation of the stagnation points

Consider

$$\{x_{3,4}, y_{3,4}\} = \left\{\pm\cos^{-1}\sqrt{\left(\phi - 1 - \frac{3q}{2} - \frac{1}{2}\sqrt{9q^2 - 24\beta q}\right)/\phi}, 0\right\}.$$

These critical points lie along the longitudinal axis. The Jacobian at these critical points is

$$J|_{\{x_{3,4},y_{3,4}\}} = \begin{bmatrix} \frac{\partial f}{\partial x} & 0 \\ 0 & -\frac{\partial f}{\partial x} \end{bmatrix},$$

where

$$\frac{\partial f}{\partial x} = \left(\frac{3\phi}{\left(\frac{3q}{2}+\frac{1}{2}\sqrt{9q^2-24\beta q}\right)^2 \left(3\beta-\frac{3q}{2}-\frac{1}{2}\sqrt{9q^2-24\beta q}\right)^2} \right.$$
$$\times \left(\sqrt{\frac{\phi-1-\frac{3q}{2}-\frac{1}{2}\sqrt{9q^2-24\beta q}}{\phi}} \right)$$
$$\times \left(\sqrt{\frac{1+\frac{3q}{2}+\frac{1}{2}\sqrt{9q^2-24\beta q}}{\phi}} \right)$$
$$\times \left((q-\beta)\left(\frac{3q}{2}+\frac{1}{2}\sqrt{9q^2-24\beta q}\right)^2 \right.$$
$$\left. \left. -4\beta q\left(\frac{3q}{2}+\frac{1}{2}\sqrt{9q^2-24\beta q}\right)+6\beta^2 q \right) \right),$$

and the eigenvalues are given by

$$\lambda_{3,4} = \pm \frac{3}{\left(\frac{3q}{2}+\frac{1}{2}\sqrt{9q^2-24\beta q}\right)^2 \left(3\beta-\frac{3q}{2}-\frac{1}{2}\sqrt{9q^2-24\beta q}\right)^2}$$
$$\times \sqrt{\phi\left(1+\frac{3q}{2}+\frac{1}{2}\sqrt{9q^2-24\beta q}\right)-\left(1+\frac{3q}{2}+\frac{1}{2}\sqrt{9q^2-24\beta q}\right)^2}$$
$$\times \left((q-\beta)\left(\frac{3q}{2}+\frac{1}{2}\sqrt{9q^2-24\beta q}\right)^2 - 4\beta q\left(\frac{3q}{2}+\frac{1}{2}\sqrt{9q^2-24\beta q}\right)+6\beta^2 q \right). \quad (21)$$

From Eq. (21), we note that a discussion about these critical points is only possible for negative β. Since negative β is of no physical interest, we will not proceed further.

2.1.5. Classification and bifurcation of the critical points

The critical points are $x = (2n-1)\pi/2$ with

$$q > -\frac{1}{3}\left(\frac{(1-\phi)^2}{1-\phi+2\beta}\right),$$

where $n \in \mathbb{Z}$. As in the previous section, a degenerate fixed point bifurcates to saddle nodes on the longitudinal axis for

$$-1+\phi < q < -\frac{1}{3}\frac{(1-\phi)^2}{1-\phi+2\beta}.$$

In the case when q approaches

$$q_{c_2} = -\frac{1}{3}\frac{(1-\phi)^2}{1-\phi+2\beta},$$

the saddle nodes of adjacent waves join together below the wave troughs, therefore the critical points merge on $x = (2n-1)\pi/2$ for $q = q_{c_2}$. This join of the critical points produces degenerate points with six heteroclinic connections. The degenerate points bifurcate on the y branch at $x = (2n-1)\pi/2$ with $q > q_{c_2}$ and change to saddle nodes.

Critical points

$$\{x_{5,6},y_{5,6}\} = \left\{ \frac{(2n-1)\pi}{2}, \right.$$
$$\left. \pm\sqrt{\frac{(3q+1-\phi)(1-\phi)^2+6\beta q(1-\phi)}{3(q+1-\phi)}} \right\}$$

lie vertically below the wave troughs. The Jacobian is given by

$$J|_{\{x_{5,6},y_{5,6}\}} = \begin{bmatrix} 0 & \frac{\partial f}{\partial y} \\ \frac{\partial g}{\partial x} & 0 \end{bmatrix},$$

where

$$\frac{\partial f}{\partial y} = \pm\frac{(q+1-\phi)}{((\phi-1)^3-3\beta(\phi-1)^2)}$$
$$\times \sqrt{\frac{3(3q+1-\phi)(\phi-1)^2-18\beta q(\phi-1)}{q+1-\phi}},$$
$$\frac{\partial g}{\partial x} = \mp\frac{\phi}{3(1-\phi)^2(3\beta+1-\phi)^2(q+1-\phi)}$$
$$\times \sqrt{\frac{(3q+1-\phi)(\phi-1)^2+6\beta q(1-\phi)}{3(q+1-\phi)}}$$
$$\times [2h^4-18\beta^2q^2+12\beta h^3-36\beta^2 qh],$$

with eigenvalues

$$\lambda_{5,6} = \pm\left(\frac{\sqrt{6\phi(q+1-\phi)(1-\phi)\left[(3q+1-\phi)(1-\phi)^2+6\beta q(1-\phi)\right]}}{3(1-\phi)^{5/2}(3\beta+1-\phi)^{3/2}(q+1-\phi)}\right) \times \sqrt{(1-\phi)^4-9\beta^2q^2+6\beta(1-\phi)^3-18\beta^2q(1-\phi)}. \quad (22)$$

Qualitative changes of the critical points for $q \geq -(1-\phi)^2/(3[1-\phi+2\beta])$ on $x=(2n-1)\pi/2$ take place as follows:

I) $P_{56}=0$ and $d_{56}=0$ when $q=q_{c_2}$, therefore the critical point is degenerate. Since $J|_{\{x_{5,6},y_{5,6}\}}=0$ with $q=q_{c_2}$, therefore the degeneracy is non-simple; see Fig. 2(b).

II) $P_{56}=0$ and $d_{56}<0$ when $q>-(1-\phi)^2/(3[1-\phi+2\beta])$, therefore the critical points are saddle nodes; see Fig. 2(c).

A bifurcation diagram in the y–q plane with the variation of β is shown in Fig. 2.

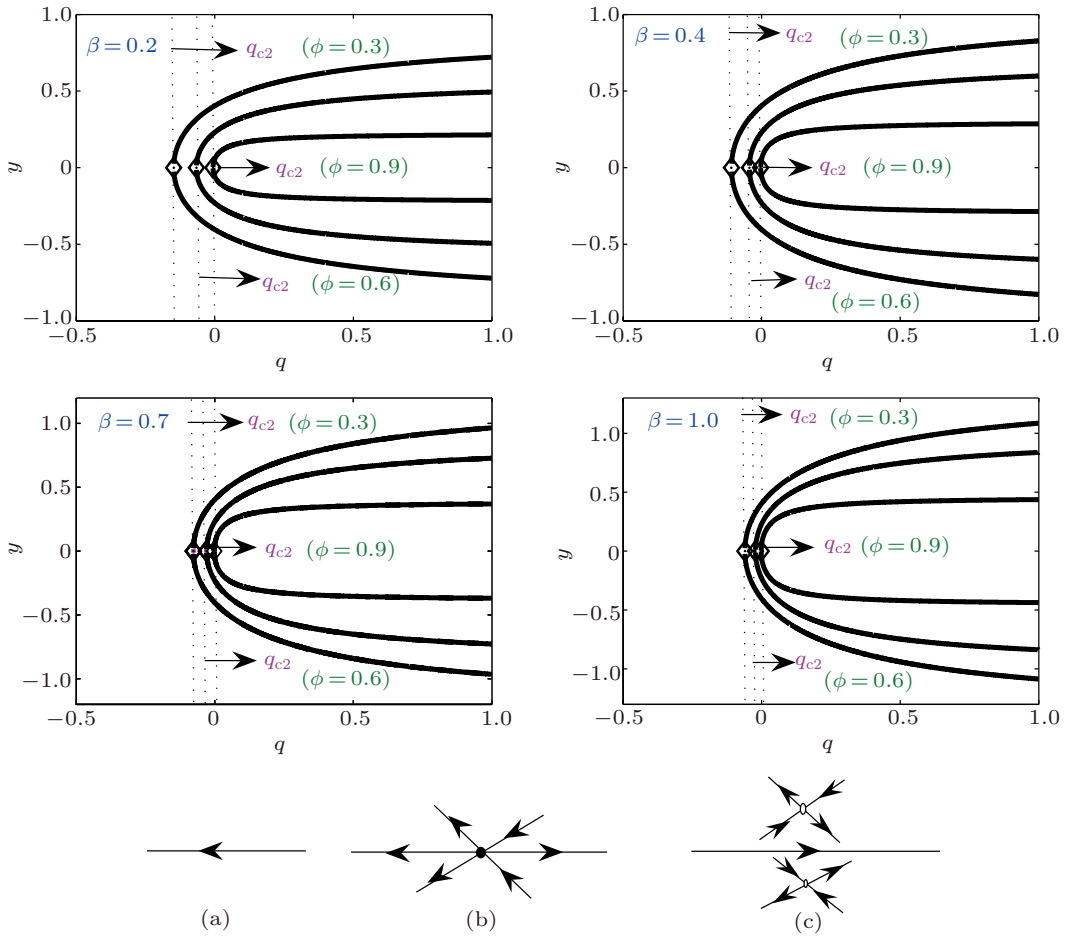


Fig. 2. (color online) Local bifurcations for wave troughs at $x=(2n-1)\pi/2$ with $q>-(1-\phi)^2/(3[1-\phi+2\beta])$ for different values of ϕ and pictorial changes: (a) $q<-(1-\phi)^2/(3[1-\phi+2\beta])$, (b) $q=-(1-\phi)^2/(3[1-\phi+2\beta])$, (c) $q>-(1-\phi)^2/(3[1-\phi+2\beta])$.

2.1.6. Global bifurcation and streamline patterns

The vector field associated with $y=0$ is

$$\{\dot{x},\dot{y}\}=\left\{\frac{3qh+h^2+6\beta q}{2h^2+6\beta h},0\right\},$$

from which $\xi=q+h^2/(3h+6\beta)$. The critical conditions crop up at the wave crests $x=n\pi$ and troughs $x=(2n-1)\pi/2$. The global bifurcation curves are given by $f(\boldsymbol{x},\boldsymbol{\alpha})=\xi=0$, so we have

$$\xi|_{(x=n\pi)}=q+\frac{1}{(3+6\beta)}=0,$$

$$\xi|_{(x=(2n-1)\pi/2)}=q+\frac{(1-\phi)^2}{(3(1-\phi)+6\beta)}=0.$$

The global bifurcation diagram in the ϕ–q parameter space with the variation of β contains the following set of curves:

$$M=\left\{(\phi,q)|0<\phi<1,q=\frac{-1}{(3+6\beta)}\right\}, \quad (23)$$

$$N=\left\{(\phi,q)|0<\phi<1,q=\frac{(1-\phi)^2}{(3(1-\phi)+6\beta)}\right\}. \quad (24)$$

Along the bifurcation curve M, an isolated non-hyperbolic degenerate point exists below the wave crest, which is also non-simple. Whereas along the bifurcation curve N, the associated critical points join together below the wave troughs and form connections of non-simple degenerate points. The critical points that amalgamate on N produce a degenerate saddle having six heteroclinic paths. Figure 3 is constructed to show the bifurcation curves.

The region of the peristaltic flow is divided as follows:

Region I: backward flow, where all the flows go in the opposite direction to the flow.

Region II: trapping, where saddles are connected by heteroclinic connections and the interaction of two vortices with opposite rotations exist in the flow.

Region III: augmented flow, where the eddies below the wave crests merge and form heteroclinic connections with their neighbors, and part of the fluid is able to flow through the centerline in the flow direction.

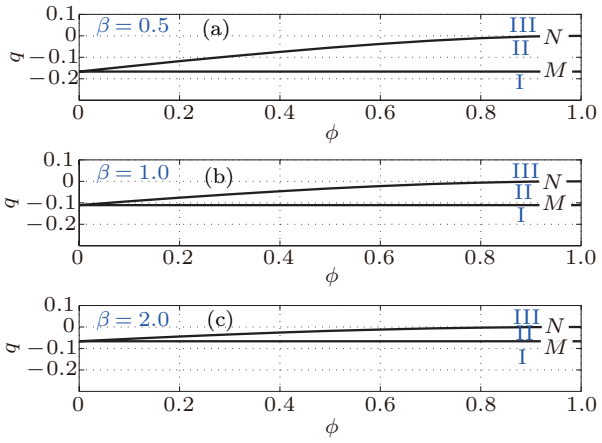


Fig. 3. (color online) Global bifurcations for planar flow with the variation of β: (a) $\beta = 0.5$, (b) $\beta = 1.0$, (c) $\beta = 2.0$; region I: backward flow, region II: trapping, region III: augmented flow.

2.2. Axisymmetric flow

Now we consider the peristaltic motion of an incompressible Newtonian fluid in an axisymmetric tube with flexible walls. The tube wall in cylindrical coordinates $(\overline{R},\overline{Z})$ is expressed as

$$\overline{H}_a(\overline{Z},\bar{t}) = R_a - a\left[1-\cos^2\left(\frac{\pi}{\lambda}(\overline{Z}-c\bar{t})\right)\right], \tag{25}$$

in which R_a is the tube radius and a, λ, c are the same as those defined for the planar case.

In the laboratory frame $(\overline{X},\overline{Y})$, the governing equations can be written as

$$\frac{1}{\overline{R}}\frac{\partial}{\partial\overline{R}}(\overline{R}\overline{V}_{\overline{R}}) + \frac{\partial\overline{V}_{\overline{Z}}}{\partial\overline{Z}} = 0, \tag{26}$$

$$\rho\left(\frac{\partial}{\partial\bar{t}} + \overline{V}_{\overline{R}}\frac{\partial}{\partial\overline{X}} + \overline{V}_{\overline{Z}}\frac{\partial}{\partial\overline{Y}}\right)\overline{V}_{\overline{R}} = -\frac{\partial\overline{P}}{\partial\overline{R}} + \mu\left(\frac{\partial}{\partial\overline{R}}\left(\frac{1}{\overline{R}}\frac{\partial}{\partial\overline{R}}(\overline{R}\overline{V}_{\overline{R}})\right) + \frac{\partial^2\overline{V}_{\overline{R}}}{\partial\overline{Z}^2}\right), \tag{27}$$

$$\rho\left(\frac{\partial}{\partial\bar{t}} + \overline{V}_{\overline{R}}\frac{\partial}{\partial\overline{X}} + \overline{V}_{\overline{Z}}\frac{\partial}{\partial\overline{Y}}\right)\overline{V}_{\overline{Z}} = -\frac{\partial\overline{P}}{\partial\overline{Z}} = +\mu\left(\frac{1}{\overline{R}}\frac{\partial}{\partial\overline{R}}\left(\overline{R}\frac{\partial\overline{V}_{\overline{Z}}}{\partial\overline{R}}\right) + \frac{\partial^2\overline{V}_{\overline{Z}}}{\partial\overline{Z}^2}\right), \tag{28}$$

where ρ is the fluid density, $\overline{V}_{\overline{R}}$ and $\overline{V}_{\overline{Z}}$ are respectively the velocity components in $\overline{R}$ and $\overline{Z}$ directions, and $\bar{t}$ is the time.

To perform the steady analysis, we switch from laboratory frame $(\overline{R},\overline{Z})$ to wave frame $(\bar{r},\bar{z})$ moving with wave speed c. The following transformations between the two frames are used:

$$\bar{z} = \overline{Z} - c\bar{t}, \quad \bar{r} = \overline{R}, \quad \overline{v}_{\bar{z}} = \overline{V}_{\overline{Z}} - c, \quad \overline{v}_{\bar{r}} = \overline{V}_{\overline{R}},$$
$$\overline{p}(\bar{r},\bar{z}) = \overline{P}(\overline{R},\overline{Z},\bar{t}), \tag{29}$$

where $\overline{v}_{\bar{r}}$ and $\overline{v}_{\bar{z}}$ are the corresponding velocity components in the wave frame. By virtue of the dimensionless parameters

$$z = \frac{\pi\bar{z}}{\lambda}, \quad r = \frac{\bar{r}}{R_a}, \quad v_z = \frac{\overline{v}_{\bar{z}}}{c}, \quad v_r = \frac{\overline{v}_{\bar{r}}}{\epsilon_a c}, \quad t = \frac{\pi c\bar{t}}{\lambda},$$
$$p = \frac{\epsilon_a R_a\overline{p}}{\mu c}, \quad h_a = \frac{\overline{h}_a}{R_a}, \tag{30}$$

and with the help of the stream function

$$v_r = -\frac{1}{r}\frac{\partial\psi_a}{\partial z}, \quad v_z = \frac{1}{r}\frac{\partial\psi_a}{\partial r}, \tag{31}$$

we find that equation (26) is identically satisfied, whereas the Navier–Stokes equations (27) and (28), after the cross differentiation for eliminating the pressure gradient, take the same form as that in Ref. [31]

$$\epsilon_a Re_a\left[\frac{\partial\left(\psi_a, \nabla_a^2\psi_a/r^2\right)}{\partial(r,z)}\right] = \frac{1}{r}\nabla_a^2(\nabla_a^2\psi_a). \tag{32}$$

The dimensionless form of the tube surface is

$$h_a(z) = 1 - \phi_a\left(1-\cos^2 z\right). \tag{33}$$

The wave number ϵ_a, Reynolds number Re_a, amplitude ratio ϕ_a, and modified Laplacian ∇_a^2 are defined as

$$\epsilon_a = \frac{\pi R_a}{\lambda}, \quad Re_a = \frac{\rho c R_a}{\mu}, \quad \phi_a = \frac{a}{R_a}(<1),$$
$$\nabla_a^2 = \epsilon_a^2\frac{\partial^2}{\partial z^2} + \frac{\partial^2}{\partial r^2} - \frac{1}{r}\frac{\partial}{\partial r}. \tag{34}$$

By employing the long wavelength and the low Reynolds number assumptions, equation (32) reduces to a similar form as obtained by Ref. [31]

$$\nabla_a^2(\nabla_a^2\psi) = 0. \tag{35}$$

The dimensionless volume flow rate and boundary conditions in the wave frame are

$$\psi_a = 0, \quad \frac{\partial}{\partial r}\left(\frac{1}{r}\frac{\partial\psi_a}{\partial r}\right) = 0, \quad \text{at } r = 0, \tag{36a}$$

$$\psi_a = q_a, \quad \frac{1}{r}\frac{\partial\psi_a}{\partial r} + \beta_a\frac{\partial}{\partial r}\left(\frac{1}{r}\frac{\partial\psi_a}{\partial r}\right) = -1, \quad \text{at } r = h_a, \tag{36b}$$

$$q_a = \int_0^{h_a}\frac{\partial\psi_a}{\partial r}\,\mathrm{d}r = \psi_a(h_a) - \psi_a(0). \tag{37}$$

Here β_a $(= \eta/R_a)$ is the dimensionless slip parameter, h_a is the dimensionless form of the peristaltic wall, and q_a is the mean flow rate in the wave frame.

2.2.1. Solution of the problem

The solution of Eq. (35) subject to boundary conditions (36a) and (36b) is

$$\psi_a = \frac{1}{(h_a+4\beta_a)}\left[\left(\frac{2q_a}{h_a} + \frac{h_a}{2} + \frac{4q_a\beta_a}{h_a^2}\right)r^2 - \left(\frac{q_a}{h_a^3} + \frac{1}{2h_a}\right)r^4\right]. \tag{38}$$

2.2.2. Dynamical system approach to the flow field

We can write the present problem as a system of nonlinear differential equations by using the relations

$$\dot{z} = v_z = \frac{1}{r}\frac{\partial\psi_a}{\partial r}$$

and

$$\dot{r} = v_r = -\frac{1}{r}\frac{\partial \psi_a}{\partial z}.$$

Invoking Eq. (38), we have

$$\begin{aligned}\dot{z} &= \frac{1}{h_a^3(h_a+4\beta_a)}\left[h_a^4 - 4q_a r^2 + h_a^2\left(4q_a - 2r^2\right) + 8h_a q_a \beta_a\right] \\ &= l(z,r,\boldsymbol{\alpha}_a), \qquad (39)\\ \dot{r} &= r\frac{\partial h_a}{\partial z}\frac{1}{h_a^4(h_a+4\beta_a)^2}[4h_a^3 q_a - h_a\left(h_a^2+4q_a\right)r^2 \\ &\quad -2(h_a^4+6q_a r^2+h_a^2\left(-10q_a+r^2\right))\beta_a + 32\beta_a^2 q_a h_a] \\ &= m(z,r,\boldsymbol{\alpha}_a), \qquad (40)\end{aligned}$$

where $\boldsymbol{\alpha}_a = [\phi_a, q_a, \beta_a]$, $-\infty < z < \infty$, $-h_a < r < h_a$, and the amplitude ratio $0 < \phi_a < 1$.

For the critical points, we set $l(z,r,\boldsymbol{\alpha}_a) = 0 = m(z,r,\boldsymbol{\alpha}_a)$ and use the same technique as applied for the planar case. The critical points are given by

$$1)\ \{z_{1,2}, r_{1,2}\} = \left\{n\pi, \pm\sqrt{\frac{4q_a(2\beta_a+1)+1}{2(2q_a+1)}}\right\},$$

$$2)\ \{z_{3,4}, r_{3,4}\} = \left\{\pm\cos^{-1}\sqrt{\frac{\phi_a - 1 - \frac{3q_a}{2} - \frac{1}{2}\sqrt{9q_a^2 - 24\beta_a q_a}}{\phi_a}}, 0\right\},$$

$$3)\ \{z_{5,6}, r_{5,6}\} = \left\{\frac{(2n-1)\pi}{2}, \pm\sqrt{\frac{(4q_a+(\phi_a-1)^2)(\phi_a-1)^2 - 8\beta_a q_a(\phi_a-1)}{2(2q_a+(\phi_a-1)^2)}}\right\}.$$

Next we present the qualitative classification and discussion of the critical points. We also present a discussion about the critical values with local and global bifurcation diagrams for the critical points.

2.2.3. Classification and bifurcation of the critical points

Consider

$$\{z_{1,2}, r_{1,2}\} = \left\{n\pi, \pm\sqrt{\frac{4q_a(2\beta_a+1)+1}{2(2q_a+1)}}\right\},$$

where $n \in \mathbb{Z}$. These critical points lie on a vertical line below the wave crests. The Jacobian at these critical points is

$$J_a|_{\{z_{1,2},r_{1,2}\}} = \begin{bmatrix} 0 & \frac{\partial l}{\partial r} \\ \frac{\partial m}{\partial z} & 0 \end{bmatrix}, \qquad (41)$$

where

$$\begin{aligned}\frac{\partial l}{\partial r} &= \mp\frac{4}{4\beta_a+1}(2q_a+1)\sqrt{\frac{4q_a(2\beta_a+1)+1}{2(2q_a+1)}}, \\ \frac{\partial m}{\partial z} &= \mp\frac{\phi_a\left[-1+2(-3+4q_a+8q_a^2)\beta_a + 8q_a(7+10q_a)\beta_a^2\right]}{(2q+1)(4\beta+1)^2} \\ &\quad \times\sqrt{\frac{4q_a(2\beta_a+1)}{2(2q_a+1)}},\end{aligned}$$

and the eigenvalues are given by

$$\begin{aligned}\lambda_{1,2}^a = &\pm\left(\frac{\sqrt{-(4q_a+2)(4q_a(2\beta_a+1)+1)(4\beta_a+1)\phi_a}}{(2q_a+1)(4\beta_a+1)^2}\right) \\ &\times\left(\sqrt{1-2(-3+4q_a+8q_a^2)\beta_a - 8q_a(7+10q_a)\beta_a^2}\right). \qquad (42)\end{aligned}$$

To discuss the qualitative changes, we again take $-1 < q_a < 1$. The changes occur in the following way:

a) $p_{12}^a = 0$ and $d_{12}^a < 0$ when $-1/2 < q_a < -1/(4+8\beta_a)$. The critical point is a co-dimension-two saddle as it depends on β_a and q_a; see Fig. 4(a).

b) $p_{12}^a = 0$ and $d_{12}^a = 0$ at $q_a = q_{c_1}^a = -1/(4+8\beta_a)$ and the critical point is a non-simple degenerate point because $J_a|_{\{z_{1,2},r_{1,2}\}} = 0$, see Fig. 4(b).

c) $p_{12}^a = 0$ and $d_{12}^a > 0$ when $q_a > -1/(4+8\beta)$, therefore each critical point is a center; see Fig. 4(c).

2.2.4. Classification and bifurcation of the critical points ($\beta \le 0$)

The critical points

$$\{z_{3,4}, r_{3,4}\} = \left\{\pm\cos^{-1}\left(\sqrt{\frac{2^{1/3}\sqrt{q_a}\left(\sqrt{q_a}+\sqrt{3}\sqrt{-q_a}\right)}{\left(-9q_a\beta_a+\sqrt{3}\sqrt{4q_a^3+27q_a^2\beta_a^2}\right)^{1/3}} - 1 + \phi_a - \frac{\left(\sqrt{q_a}-\sqrt{3}\sqrt{-q_a}\right)\left(-9q_a\beta_a+\sqrt{3}\sqrt{4q_a^3+27q_a^2\beta_a^2}\right)^{1/3}}{18^{1/3}\sqrt{q_a}}}\right), 0\right\}$$

lie along the longitudinal axis. The Jacobian at these critical points is

$$J|_{\{z_{3,4},r_{3,4}\}} = \begin{bmatrix} \frac{\partial l}{\partial z} & 0 \\ 0 & -\frac{1}{2}\frac{\partial l}{\partial z} \end{bmatrix},$$

where

$$\frac{\partial l}{\partial z} = 4\frac{\partial h_a}{\partial z}\left(\frac{-2q_a h_a^2 + h_a^3\beta_a - 10q_a h_a\beta_a - 16q_a\beta_a^2}{h_a^3(h_a+4\beta_a)^2}\right),$$

and the eigenvalues are given by

$$\lambda_3^a = \frac{\partial l}{\partial z}, \quad \lambda_4^a = -\frac{1}{2}\frac{\partial l}{\partial z}. \qquad (43)$$

Here we would again mention that the existence of these critical points is subject to negative values of β_a and therefore these critical points are of no physical interest.

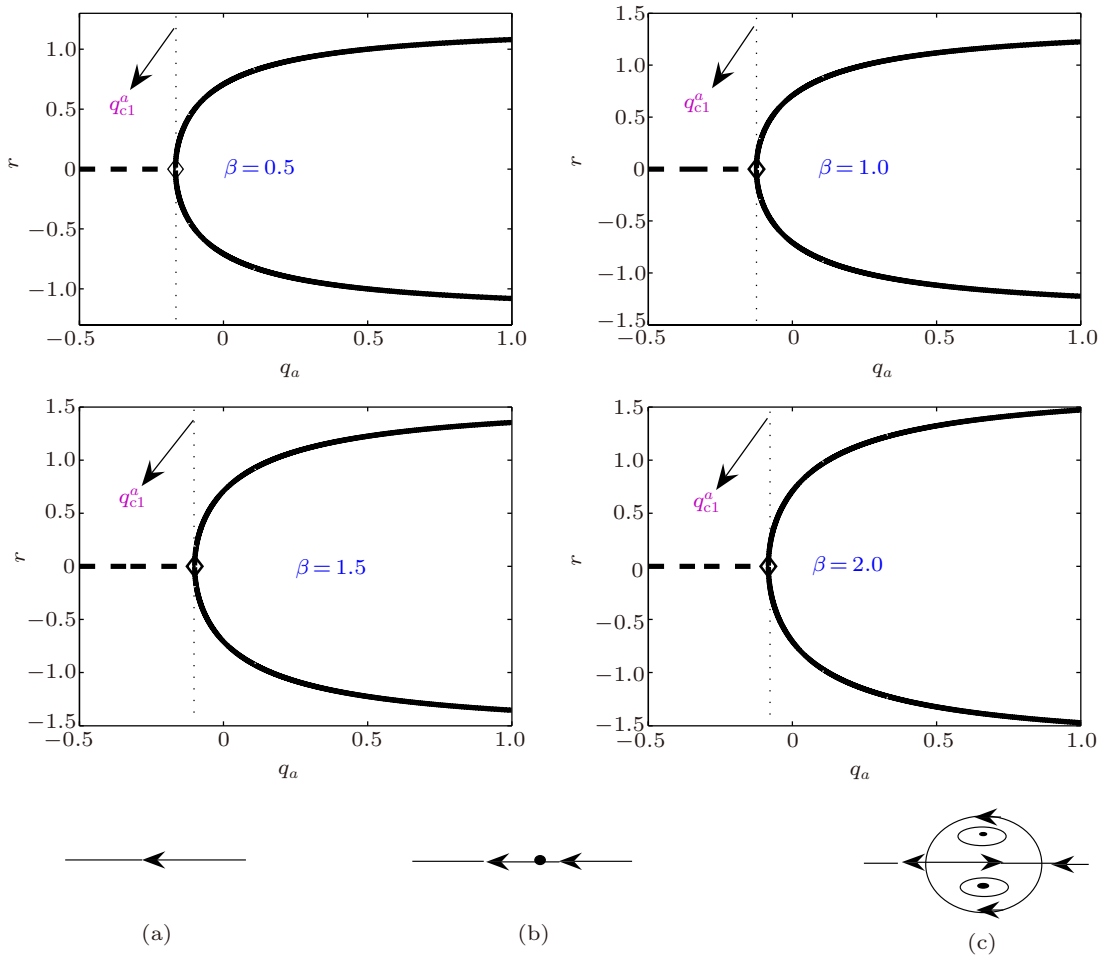


Fig. 4. (color online) Local bifurcation for wave crest $z = n\pi$, $n \in \mathbb{Z}$ and pictorial topological changes: (a) $q_a < -1/(4+8\beta_a)$, (b) $q_a = -1/(4+8\beta_a)$, (c) $q_a > -1/(4+8\beta_a)$.

2.2.5. Classification and bifurcation of the critical points

Now take $z = (2n-1)\pi/2$ with $q_a \geq -(1-\phi_a)^3/[4(1-\phi_a)+8\beta_a]$, where $n \in \mathbb{Z}$. As previously mentioned, a degenerate fixed point bifurcates to saddle nodes on the longitudinal axis for

$$-\frac{1}{4+8\beta_a} < q_a < -\frac{(1-\phi_a)^3}{4(1-\phi_a)+8\beta_a}.$$

As q_a approaches $q^a_{c_2} = -(1-\phi_a)^3/[4(1-\phi_a)+8\beta_a]$, the saddle nodes of contiguous waves coalesce below the wave troughs. The critical points merge on $z = (2n-1)\pi/2$ with $q_a = q^a_{c_2}$, this produces degenerate points with six heteroclinic connections. For $q_a > q^a_{c_2}$, the degenerate points bifurcate on the r branch at $z = (2n-1)\pi/2$ and change to saddle nodes.

Critical points

$$\{z_{5,6}, r_{5,6}\} = \left\{ \frac{(2n-1)\pi}{2}, \pm\sqrt{\frac{(4q_a+(\phi_a-1)^2)(\phi_a-1)^2-8\beta_a q_a(\phi_a-1)}{2(2q_a+(\phi_a-1)^2)}} \right\}$$

lie on the vertical below the wave trough. The Jacobian is given by

$$J|_{\{z_{5,6},r_{5,6}\}} = \begin{bmatrix} 0 & \dfrac{\partial l}{\partial r} \\ \dfrac{\partial m}{\partial z} & 0 \end{bmatrix},$$

where

$$\frac{\partial l}{\partial r} = \pm \frac{4\left(2q_a+(\phi_a-1)^2\right)}{(1-\phi_a+4\beta_a)(\phi_a-1)^3}\sqrt{\frac{\left(4q_a+(\phi_a-1)^2\right)(\phi_a-1)^2-8q_a\beta_a(\phi_a-1)}{2\left(2q_a+(\phi_a-1)^2\right)}},$$

$$\frac{\partial m}{\partial z} = \pm\left(\frac{2\phi_a\left[-16q_a\beta_a^2\left(2q_a+3(\phi_a-1)^2\right)+2\beta_a\left(2q_a-3(\phi_a-1)^2\right)(\phi_a-1)^3+(\phi_a-1)^6\right]}{2\left(2q_a+(\phi_a-1)^2\right)(\phi_a-1)^3(\phi_a-1-4\beta_a)}\right)$$

$$\times \left(\sqrt{\frac{\left(4q_a + (\phi_a - 1)^2\right)(\phi_a - 1)^2 - 8q_a\beta_a(\phi_a - 1)}{2\left(2q_a + (\phi_a - 1)^2\right)}} \right),$$

with eigenvalues

$$\lambda_{5,6} = \pm \left(\frac{\sqrt{2\phi_a\left(2q_a + (\phi_a - 1)^2\right)\left\{\left(4q_a + (\phi_a - 1)^2\right)(\phi_a - 1)^2 - 8q_a\beta_a(\phi_a - 1)\right\}}}{(\phi_a - 1)^3(4\beta_a + 1 - \phi_a)^{3/2}\left(2q_a + (\phi_a - 1)^2\right)} \right)$$
$$\times \sqrt{(\phi_a - 1)^6 - 16\beta_a^2 q_a\left(2q_a + 3(\phi_a - 1)^2\right) + 2\beta_a\left(2q_a - 3(\phi_a - 1)^2\right)(\phi_a - 1)^3}. \quad (44)$$

Qualitative changes of the critical points take place as follows:

c1) $P_{56}^a = 0$ and $d_{56}^a = 0$ at $q_a = q_{c_2}^a$ and the critical point is non-simple degenerate because $J|_{\{z_{5,6}, r_{5,6}\}} = 0$; see Fig. 5(b);

c2) $P_{56}^a = 0$ and $d_{56}^a < 0$ when $q_a > -(1-\phi_a)^3/[4(1-\phi_a) + 8\beta_a]$, therefore the critical points are saddle nodes; see Fig. 5(c).

A bifurcation diagram for the r–q_a plane is traced with ϕ_a and β_a fixed; see Fig. 5.

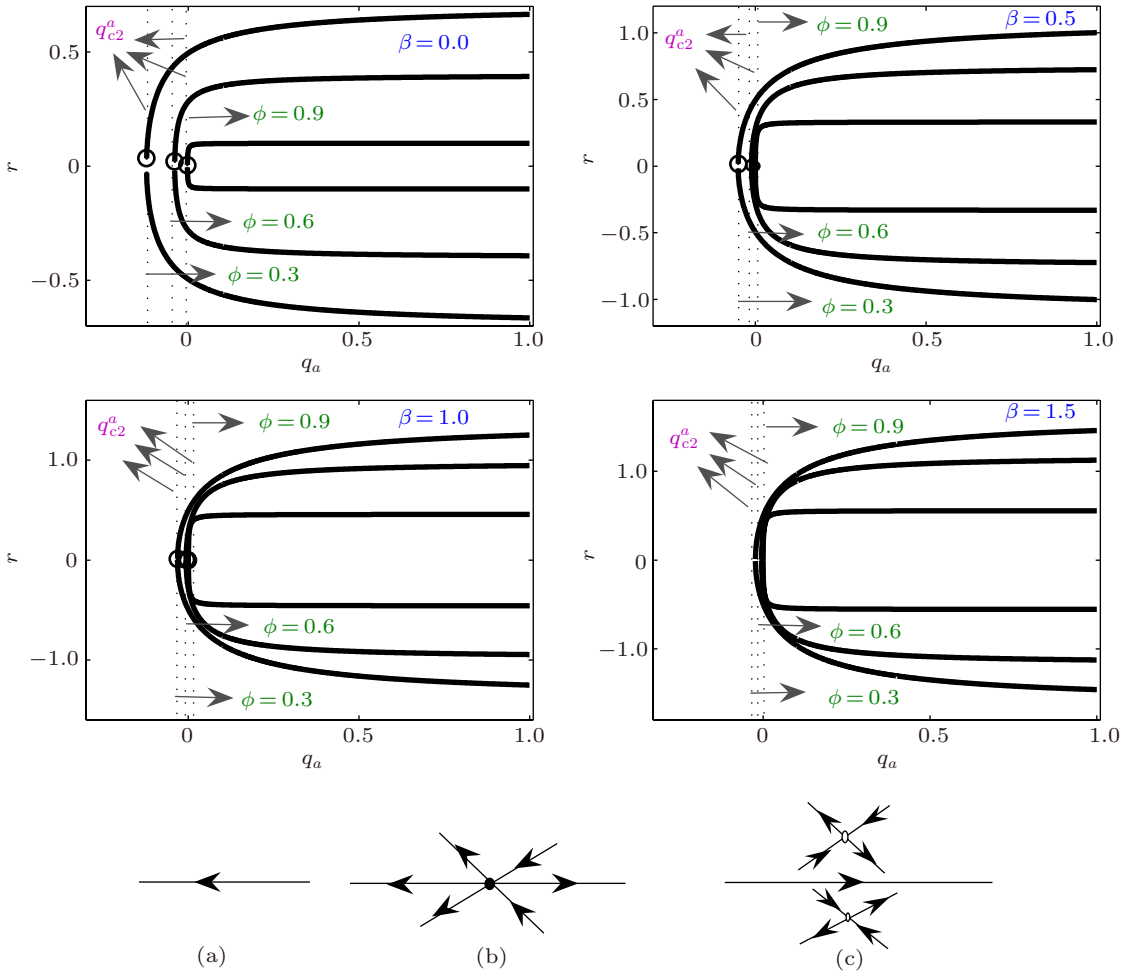


Fig. 5. (color online) Local bifurcation for wave troughs $z = (2n-1)\pi/2$ with $q_a > -(1-\phi_a)^3/(4(1-\phi_a) + 8\beta_a)$ with different values of ϕ_a and pictorial changes: (a) $q_a < -(1-\phi_a)^3/(4(1-\phi_a) + 8\beta_a)$, (b) $q_a = -(1-\phi_a)^3/(4(1-\phi_a) + 8\beta_a)$, (c) $q_a > -(1-\phi_a)^3/(4(1-\phi_a) + 8\beta_a)$.

2.2.6. Global bifurcation and streamline patterns

The associated vector field for $r = 0$ is

$$\{v_z, v_r\} = \left\{ \frac{h_a^3 + 4h_a q_a + 8q_a\beta_a}{h_a^2(h_a + 4\beta_a)}, 0 \right\},$$

from which

$$\xi^a = q_a + \frac{h_a^3}{4(h_a + 2\beta_a)}.$$

The critical conditions occur at the wave crests $z = n\pi$ and troughs $z = (2n-1)\pi/2$. The bifurcation curves are given by

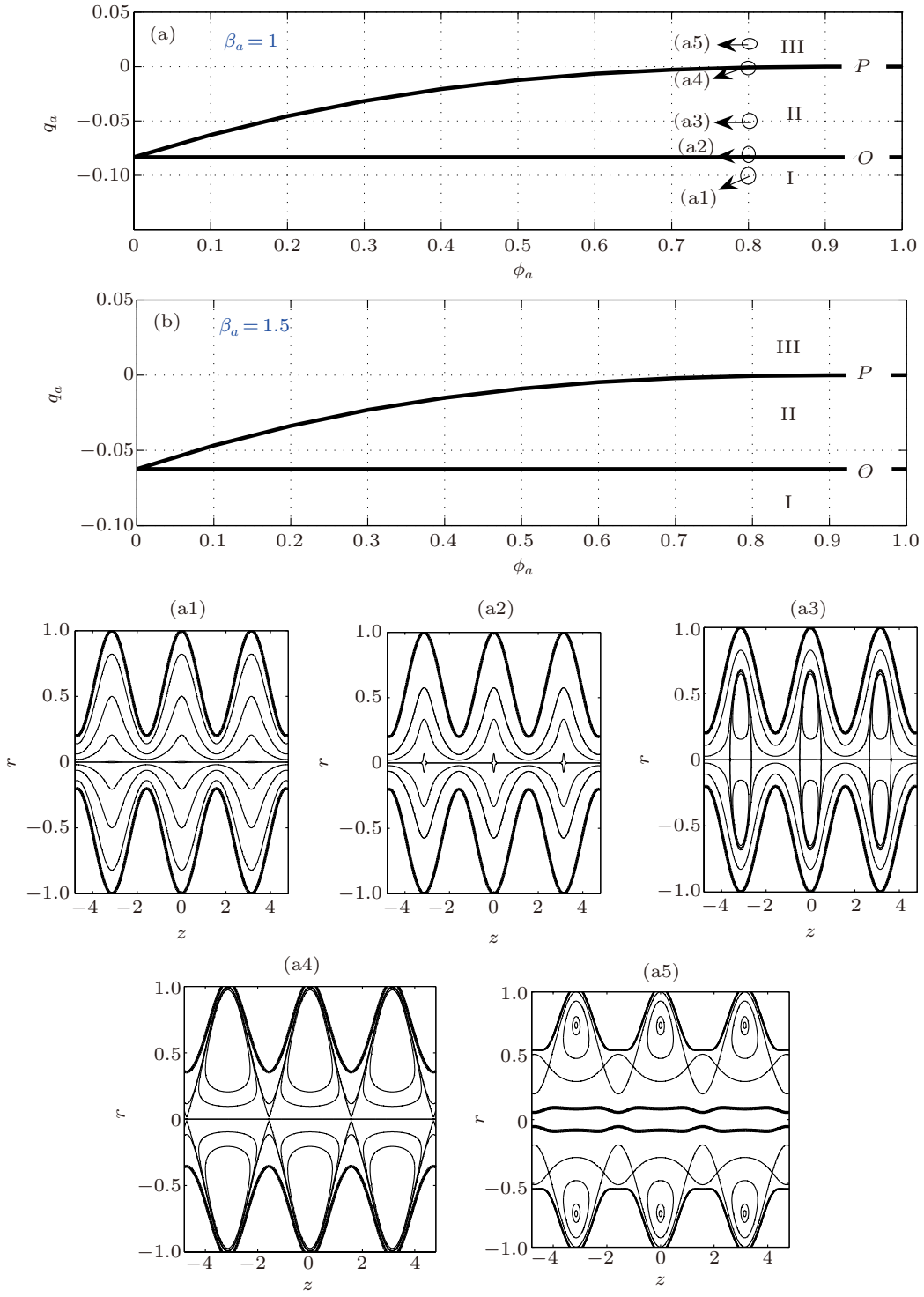


Fig. 6. (a) and (b) Global bifurcation diagrams, for axisymmetric flow, subpanels (a1)–(a5) correpond to $\phi_a = 0.6$ with different values of q_a; region I: backward flow, region II: trapping, region, III: augmented flow, (a1) $q_a = -0.1$, (a2) $q_a = -0.08$, (a3) $q_a = -0.05$, (a4) $q_a = -0$, (a5) $q_a = 0.02$.

$l(\overline{z}, \boldsymbol{\alpha}_a) = \xi^a = 0$, so we have

$$\xi^a|_{(z=n\pi)} = q_a + \frac{1}{4(1+2\beta_a)} = 0,$$

$$\xi^a|_{(z=\frac{(2n-1)\pi}{2})} = q_a + \frac{(1-\phi_a)^3}{4(1-\phi_a+2\beta_a)} = 0.$$

The global bifurcation diagram in the ϕ_a–q_a parameter space with β_a fixed contains the following curves:

$$O = \left\{ (\phi_a, q_a) | 0 < \phi_a < 1, q_a = \frac{-1}{4(1+2\beta_a)} \right\}, \quad (45)$$

$$P = \left\{ (\phi_a, q_a) | 0 < \phi_a < 1, q_a = -\frac{(1-\phi_a)^3}{4(1-\phi_a+2\beta_a)} \right\}. \quad (46)$$

Along the bifurcation curve O, an isolated non-hyperbolic de-

generate point exists below the wave crest, which is also non-simple. Whereas along the bifurcation curve P, the associated critical points join together below the wave troughs and form connections of non-simple degenerate points. The critical points that amalgamate on P produce a degenerate saddle having six heteroclinic paths. The bifurcation curves are shown in Fig. 6. Figures 6(a1)–6(a5) highlight the transitions between different values of q_a with fixed ϕ_a and β_a.

3. Results

Different flow formations occurring in the peristaltic motion are shown in Figs. 1–6. Figure 1 shows the bifurcation that occurs corresponding to the critical points $\{x_{1,2}, y_{1,2}\}$ for different values of the slip parameter. Here we observe that with the increase in the slip parameter β, the bifurcation point occurs at larger flow rates. Moreover, the vortices spread along the vertical direction. Similar observations are made in Fig. 2. The global bifurcation diagram is presented in Fig. 3. From this figure, we observe that with an increase in the slip parameter, the backward flow region expands whereas the trapping region narrows down. However, no change occurs in the augmented flow region by increasing the slip parameter. This explains the vanishing trapped bolus with an increase in the slip parameter. In fact, if one keeps increasing β for a fixed value of q, then the backward flow region expands as a result and encloses the chosen value of q. Thus, this chosen value of q, which was initially in the trapping region, now falls in the backward flow region where the trapping phenomenon is not possible.

Figures 4–6 are plotted for the axisymmetric case, and the observations in Figs. 4 and 5 are similar to those noticed in Figs. 1 and 2. Figure 6 shows the global bifurcation curves and the streamline patterns for different values of slip parameter β_a. In order to show the effects of different flow regions on the streamline patterns, we take values of the flow rate (q_a) both from inside the regions (I–III) and on the lines that separate them, and then the streamlines are drawn for the five selected values of flow rate, which are shown in Fig. 6.

The whole analysis provides the bifurcation points and the parametric ranges for different flow situations (backward flow, trapping, and augmented flow). We can draw a consequence from this analysis that if peristaltic walls are made slippery, then the trapping could be reduced, and as a result, the damage of the internal parts due to contamination, if the fluid is a chemical, could be avoided.

4. Conclusions

An analysis is performed to investigate the streamline topologies and their bifurcations for the peristaltic flow of a viscous incompressible fluid in the presence of slip at the wall of a channel/tube. The main findings are as follows.

1 The trapping region narrows down by increasing the slip parameter.

2 The backward flow region expands, whereas no changes occur in the augmented flow region by increasing β.

3 The location of the bifurcation point changes with the variation of the slip parameter.

4 Transitions between the backward flow to trapping and trapping to the augmented flow corresponds to bifurcations of co-dimension two.

5 An increase in the slip parameter accelerates the lift off of the centerline and also accelerates the flow through the center.

References

[1] Shapiro A H 1967 *National Academy of Science* Natural Research Council **1** 109

[2] Shapiro A H and Latham T W 1966 *Proc. Ann. Conf. Engng. Med. Bio.*, San Francisco, California **8** 147

[3] Weinberg S L 1970 *Ph. D. Thesis*, MIT, Cambridge MA, USA

[4] Shapiro A H, Jaffrin M Y and Weinberg S L 1969 *J. Fluid Mech.* **37** 799

[5] Ebaid A 2008 *Phys. Lett. A* **372** 4493

[6] Elshahed M and Haroun M H 2005 *Math. Probs. Engng.* **6** 663

[7] Hayat T, Ali N and Asghar S 2007 *Phys. Lett. A* **363** 397

[8] Hayat T, Ahmed N and Ali N 2008 *Commun. Nonlinear Sci. Numer. Simul.* **13** 1581

[9] Hayat T, Javed M and Ali N 2008 *Transp. Porous Med.* **74** 259

[10] Hayat T, Qureshi M U and Ali N 2009 *Appl. Math. Model.* **33** 1862

[11] Hayat T, Noreen S, Asghar S and Hendi A A 2011 *Chem. Engng. Commun.* **198** 609

[12] Hayat T and Noreen S 2012 *Chem. Engng. Commun.* **199** 512

[13] Mekheimer Kh S 2008 *Phys. Lett. A* **372** 4271

[14] Mekheimer Kh S and Elmaboud Y A 2008 *Phys. Lett. A* **372** 1657

[15] Nadeem S and Akram S 2010 *Commun. Nonlinear Sci. Numer. Simul.* **15** 312

[16] Vajravelu K, Sreenadh S and Babu V R 2005 *Appl. Math. Comput.* **169** 726

[17] Vajravelu K, Radhakrishnamacharya G and Radhakrishnamurty V 2007 *Non-Linear Mech.* **42** 754

[18] Srinivas S and Muthuraj R 2010 *Chem. Engng. Commun.* **197** 1387

[19] Abd-Alla A M, Abo-Dahab S M and Al-Shahrany 2013 *Chin. Phys. B* **22** 074702

[20] Akbar N S and Nadeem S 2013 *Chin. Phys. B* **22** 014703

[21] Ali N, Sajid M and Javed T 2011 *Chin. Phys. Lett.* **28** 014704

[22] Mehmood O U, Mustapha N and Shafie S 2012 *Appl. Math. Mech.: Engl. Ed.* **33** 1313

[23] Oswatitsch K 1958 *IUTAM Symposium on Boundary Layer Research* (Berlin: Springer-Verlag) p. 357

[24] Davey A 1961 *J. Fluid Mech.* **10** 593

[25] Lighthill M J 1963 *Laminar Boundary Layers* **2** 72

[26] Hunt J C R, Abell C J, Peterka J A and Woo H 1978 *J. Fluid Mech.* **86** 179

[27] Tobak M and Peake D J 1982 *Ann. Rev. Fluid Mech.* **14** 61

[28] Perry A E and Chong M S 1987 *Ann. Rev. Fluid Mech.* **19** 125

[29] Brons M and Hartnack J N 1999 *Phys. Fluids* **11** 314

[30] Gurcan F, Deliceoglu A and Bakker P G 2005 *J. Fluid Mech.* **539** 299

[31] Jimenez J and Sen M 2010 *Chem. Engng. Process.* **49** 704

[32] Bakker P G 1991 *Bifurcations in Flow Patterns* (Dordrecht: Kluwer Academic Publishers)

[33] Seydel R 1988 *From Equilibrium to Chaos: Practical Bifurcation and Stability Analysis* (New York: Elsevier)

[34] Perko L 2000 *Differential Equations and Dynamical Systems*, 3rd edn. (Los Alamitos: Springer-Verlag)